Heliyon 10 (2024) e24121

Contents lists available at ScienceDirect

Heliyon

journal homepage: www.cell.com/heliyon

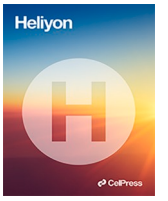

Research article

Manufacturing seamless three-dimensional woven preforms with complex shapes based on a new weaving technology

Hyun Joon Yang, Doyoung Kim, Kyeong Mo Kang, Woong-Ryeol Yu *

Department of Materials Science and Engineering (MSE) and Research Institute of Advanced Materials (RIAM), Seoul National University, Seoul, 08826, Republic of Korea

ARTICLE INFO

Keywords:
3D weaving
Z-binder interlacing
Seamless 3D woven preforms
Complex shape

ABSTRACT

A new weaving technology using a modified z-binder interlacement system was designed to demonstrate its potential for the effective, continuous, efficient, and rapid manufacturing of various three-dimensional (3D) woven structures. First, three representative 3D woven preforms were fabricated. Then, epoxy resin was transferred to a preform. The manufactured 3D woven textile-reinforced composites were investigated using micro-CT analysis, tensile tests, and bending tests to study the effect of the z-binder interlacing on the structure. Furthermore, a design rule was established that could seamlessly create complex 3D woven structures with non-uniform heights in the z-direction, such as boxes, bowls, and pyramids, demonstrating that the seamless 3D woven preform of the complex shape can be fabricated with structural integrity.

1. Introduction

Carbon fiber-reinforced plastics (CFRPs) have a high strength and stiffness-to-weight ratio; therefore, these materials can substitute, for example, metals, and they are widely used in various industries such as the automobile and aerospace industries [1–3]. Because two-dimensional (2D) fiber-reinforced plastics (FRP) have no reinforcing elements in the thickness direction, mechanical properties deteriorate in that direction. Delamination of 2D FRPs is one of the main causes of their poor mechanical properties [4,5]. Various methods, including z-pinning [6–8], stitching [9–11], tufting [6,12], resin toughening [13], and interface strengthening [14], have been employed to solve this problem; however, no complete solution has been provided. To overcome the limitations of 2D FRPs, several studies have been conducted on novel 3D preform weaving methods [15–20]. The three most representative three-dimensional (3D) woven structures are the orthogonal (ORT) structure, layer-to-layer (LTL) structure, and angle-interlock (AI) structure. Numerous studies have been carried out to evaluate and characterize the mechanical properties for these three structures [19,21–23]. In addition to these established weaving structures, research has been undertaken to explore new weaving techniques. An examination of flexural behavior was conducted through the design of a novel weaving technology, utilizing a modified heddle position system based on a self-built 3D loom, resulting in the production of four representative 3D weaving structures [18]. Subsequently, an experimental investigation was carried out to assess the low-velocity impact performance of six types of 3D woven structures [24]. Furthermore, studies have been dedicated to the development and multiscale characterization of 3D warp interlocked flax fabrics with different weave structures for composite applications [25]. Research efforts have also focused on enhancing delamination resistance and

* Corresponding author.
E-mail addresses: hyunjoon92@snu.ac.kr (H.J. Yang), rezimia@snu.ac.kr (D. Kim), bbambirra@snu.ac.kr (K.M. Kang), woongryu@snu.ac.kr (W.-R. Yu).

https://doi.org/10.1016/j.heliyon.2024.e24121
Received 3 September 2023; Received in revised form 18 October 2023; Accepted 3 January 2024
Available online 4 January 2024

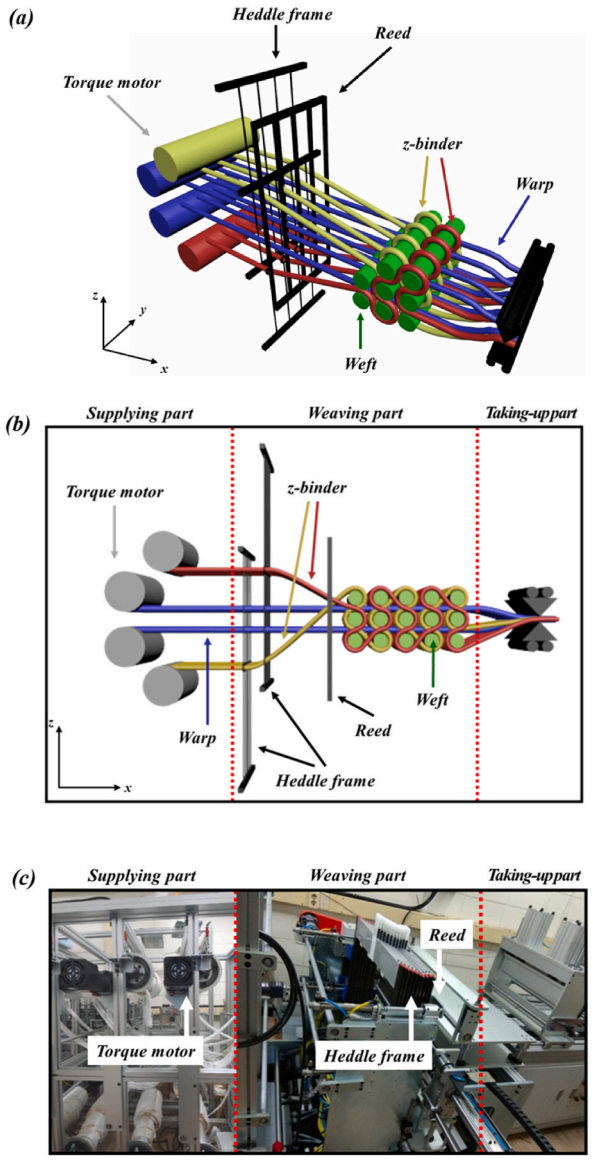

Fig. 1. Schematic representation of the new 3D weaving equipment: (a) overview, (b) individual parts in the xz-plane view, and (c) built-in machine in a laboratory [15].

out-of-plane mechanical properties through 3D fully interlaced preform weaving [26,27]. Additionally, new 3D woven ORT fabrics with improved auxeticity are currently under development for reinforced composites [28]. Various woven structures have been proposed, designed, and manufactured. The overall strength, delamination resistance [29–31], and impact performance [32–36] of the 3D woven composites were found to be excellent owing to the effect of the thick reinforcing yarn (z-binder).

CFRPs used in industries such as automobiles and aerospace must have a specific structural shape depending on the usage. Presently, 2D carbon fiber reinforcements in the form of fabrics are laminated for this purpose and then placed into a mold of a specific structure to make a composite material [31,37–44]. A limitation of these technologies is that, when molds are used, problems, such as wrinkling, occur in complex shapes [44,45]. Alternatively, after these reinforcing materials assume the shape of a structure, joints are added to create a shape. In the case of creating a joint, even if the problem of complexity is solved, there are weaknesses in the joint, such as a considerably long manufacturing time and difficulty in injecting resin.

Therefore, 3D woven preforms offer the best solution for high-performance applications with complex geometries. These preforms are specially woven to fit the desired shape. It also exhibits a uniform and well-aligned fiber distribution. Previous studies have reported on seamless 3D composite manufacturing technology, but only for manufacturing of fragmented specimen. Owing to the complexity of the manufacturing technology, reports on mass production technology are also lacking [46–53]. Textile reinforcement forming [46,47] held an advantage in terms of its process simplicity and speed. However, it suffered from drawbacks such as wrinkling,

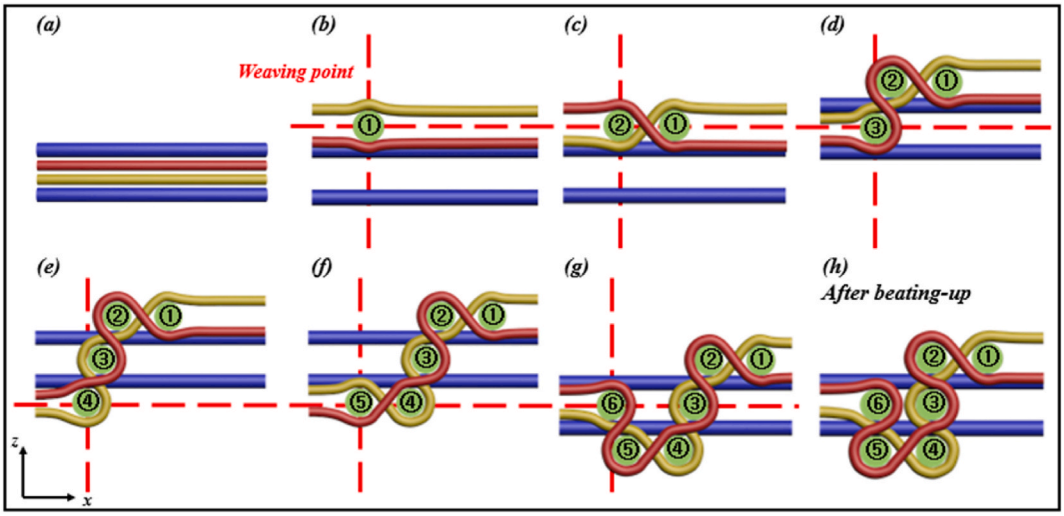

Fig. 2. An example of 3D weaving process based on the relative z-direction positioning of the warp, weft, and z-binder yarns. (a) Before weaving, (b)–(g) step by step process of inserting six weft yarns in three layers, and (h) beating-up process.

buckling, and network sliding. Surface 3D weaving [46,47] excelled in producing intricate structures with fewer defects but faced limitations for fiber plies with specific orientations, and its weaving process was time-consuming. The mathematical determination of shapes of reed wires [54] demonstrated an advantage in creating seamless and specific shapes, but it was constrained in the variety of shapes it could produce and required numerous corrections, rendering it time-intensive. Paper-folding approaches [50,52] offered the benefit of seamlessness, yet they had restrictions on the shapes achievable, resulting in uneven tension and irregular surfaces. Research has been conducted to facilitate the use of these 3D composite materials as parts; however, the complexity of the manufacturing process has not been resolved. Therefore, the development of simple, continuous, and rapid seamless 3D composite manufacturing technology has great academic and industrial significance.

In this study, the equipment for 3D woven preform manufacturing has been introduced, and the weaving mechanism has been discussed. We present three representative 3D weaving structures: through-thickness orthogonal structure (TTO), through-thickness layer-to-layer structure (TTLL), and through-thickness all-layer-interlaced structure (TTAL). These differ according to the degree of z-binder interlacing using a novel weaving mechanism. The effect of the z-binder interlacing on the structure was also analyzed. Based on the 3D woven weaving mechanism, a manufacturing process for seamless 3D complex woven preforms was established. Our weaving method, exemplified by the TTAL structure, possesses a distinct advantage in that it enables the weaving of diverse structures through careful structural design. This approach allows for the realization of complex shapes. Through the concept of weft and warp slices [48], convex and concave shapes with non-uniform heights in the z-direction were produced. This was possible because of the continuity and diversity of the TTAL structure. Furthermore, box, box lid, bowl, pyramid, and bowl-type preforms with increased complexity were produced; post-manufacturing, the internal structure was analyzed to confirm continuity. Consequently, we advocate for our method as a 'new weaving technology' with significant potential for the effective, continuous, efficient, and rapid manufacturing of various 3D woven structures.

2. Experimental

2.1. 3D weaving loom and basic weaving mechanism

Fig. 1 shows a schematic representation of the 3D weaving equipment developed in this study. Fig. 1(a) shows an overview of the 3D weaving equipment with key elements. The key elements include torque motors, heddle frames, reed, warp yarns, z-binder yarns, and weft yarns. Torque motors are used to supply warp and z-binder yarns. To ensure that all fiber yarns remain straightened during the weaving process, a torque motor provides a constant tension. The weft yarns are inserted at the corresponding positions according to the upward and downward movements of the heddle frame. Therefore, to insert the weft yarns at the desired position, the up and down movements of the heddle frame have to be set correctly. After the weft is inserted, a compact 3D woven structure is formed after the beating-up process of the reed. Fig. 1(b) shows the xz-plane view of the 3D weaving equipment in three parts: supplying, weaving, and taking-up. In the supplying part, the warp and z-binder yarns are only unwound to the length necessary for the next step of the weaving process. In the weaving part, the warp and z-binder yarns are arranged at the required positions to create the desired 3D structure. In this part, we determine whether the warp and z-binder yarns are situated above or below the weft yarn in the z-direction. The wefts are inserted between the warp and z-binder yarns, which are opened up and down using a heddle frame. The final 3D structure are determined by the relative positions of the warp, weft, and z-binder yarns along the z-direction. Finally, the preform is pulled in the x-direction in the take-up part, and the fiber volume fraction can be controlled through an appropriate pitch shift. Fig. 1(c)

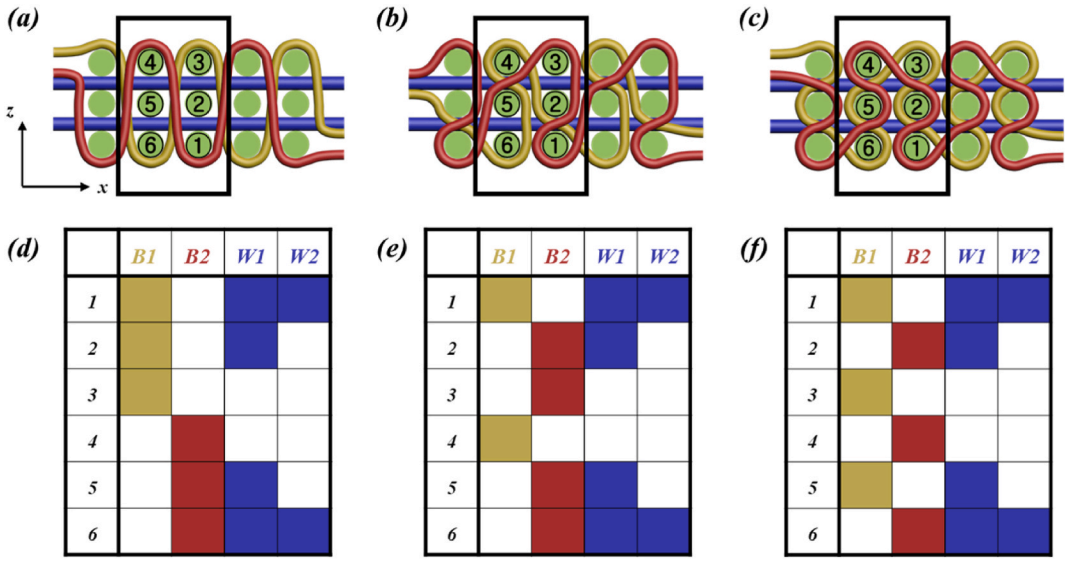

Fig. 3. Weaving process diagram of three representative 3D woven structures. 2D plane view model of (a) TTO, (b) TTLL, and (c) TTAL. The number in the model represents the weft yarns inserted in sequence. (d), (e), and (f) are the weaving process diagram of (a), (b), and (c). The number in the first column represents the weaving steps, and the 'B' and 'W' in the first row represent the z-binder and warp heddles. The numbers following the 'B' and 'W' characters represent the z-binder and warp heddles and their identification, respectively.

shows a built-in machine in a laboratory with key elements: torque motors, heddle frames, and reed.

Fig. 2 illustrates the 3D weaving process in eight steps and explains the mechanism of the 3D weaving equipment. In Fig. 2(a), prior to weaving, both heddle frames of the warp yarns and z-binder yarns are in a lowered state without any positional distinction. As weaving commences, the position of the weft yarns along the z-axis is determined by the up-and-down movement of the heddle frame. Fig. 2(b) shows the process of inserting the first weft yarn into the top layer. The weft yarn is inserted in the space between the raised yellow z-binder heddle and the lowered red z-binder heddle, known as the weaving point. This weaving point is consistent in all the weaving processes and is marked by the intersection of the red dotted line. Fig. 2(c) shows the insertion of the weft yarn with only the red z-binder heddle raised. Note that the two z-binder heddles are alternately raised during the weaving process, causing the z-binder yarns to interlace with the inserted weft yarns. Fig. 2(d) shows the insertion of the weft yarn into the middle layer. Because the weaving point remains the same, one of the two warp heddles must be raised. Fig. 2(e) shows the insertion of the weft yarn into the bottom layer. At this stage, both warp heddles are lifted. Subsequently, one weft yarn is inserted into the bottom layer (Fig. 2(f)) and another weft yarn is inserted into the middle layer (Fig. 2(g)). Fig. 2(b)–(g) show one cycle in which six weft yarns are inserted. The dense structure is produced by beating-up after each weft yarn is inserted (Fig. 2(h)).

Yarn to yarn friction is well known as the main influence on the degradation of carbon yarns [55–58]. In our study, yarn degradation caused by friction was managed by preventing unnecessary contact between yarns, maintaining appropriate tension, setting the appropriate pitch shifting, controlling the temperature and humidity in the laboratory, and reducing unnecessary stress by minimizing process variables.

2.2. Materials and 3D composites fabrication

Carbon fiber yarns (A-38, A-42, DOWAKSA, Turkey) were used, and the tensile strength of each carbon fiber yarn was 3800 MPa and 4200 MPa. Three different 3D woven structures (TTO, TTLL, and TTAL) were fabricated using warp, weft, and z-binder yarns of 6K (A-38), 12K (A-42), and 3K (A-38) carbon fibers, respectively. For the example fabrication of the seamless 3D woven preforms with complex shapes, 24K (A-42) carbon fibers were used for the warp, weft, and z-binder yarns.

The matrix consisted of epoxy resin and a hardener (Epofix; Struer, USA). The epoxy resin and hardener were mixed in a weight ratio of 25:3 at room temperature. Vacuum-assisted resin transfer molding was used to impregnate the 3D woven preforms with the epoxy resin system. After defoaming, the mixed resin was injected into a vacuum bag, and the composite was cured for 24 h at room temperature in a sealed bag.

2.3. Characterization of 3D woven composites

To analyze the fiber architecture of the 3D woven composites, micro-CT imaging (Skyscan 1275; Bruker, Belgium) was used. Datasets were reconstructed using standardized cone-beam reconstruction software (NRecon; Bruker, Belgium). For 3D visualization of the 3D woven composite, a volume rendering software (CTVox; Bruker, Belgium) was used. Through structural rendering using an analysis and visualization software (CTAn; Bruker, Belgium), the fiber volume fraction and porosity of the composite were measured.

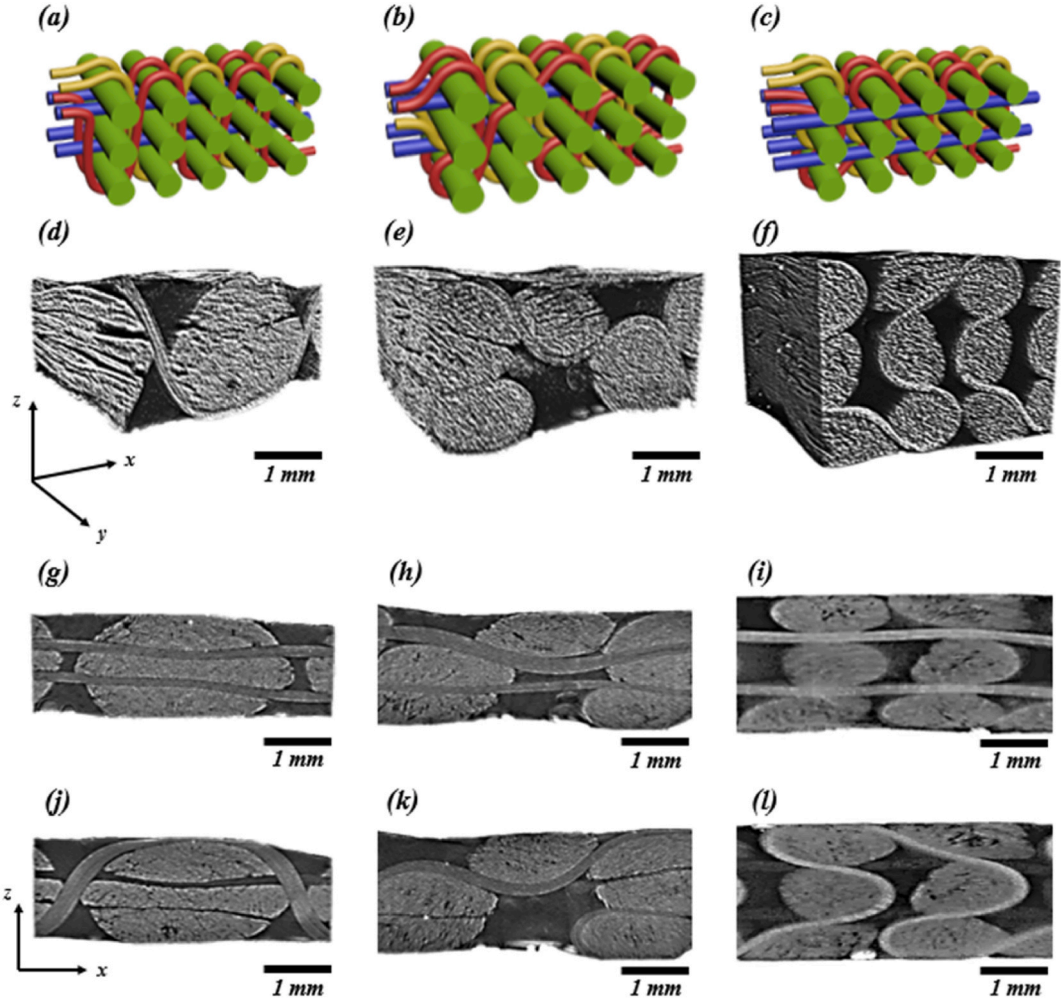

Fig. 4. Design and fabrication of three representative 3D woven structures. 3D solid model of (a) TTO, (b) TTLL, and (c) TTAL structures. 3D CT images of the fabricated 3D woven preforms with (d) TTO, (e) TTLL, and (f) TTAL structures. The xz-plane view of (g) TTO, (h) TTLL, and (i) TTAL in 3D CT images sectionized at the warps. (j), (k), and (l) are also their xz-plane view sectionized at the z-binder.

The specimens for tensile testing were prepared according to the ASTM D3039 standard ($100 \times 15 \times 2\ mm^3$). End tabs, each with a length of 20 mm, were attached to both ends of the specimen using an epoxy adhesive (DP460; 3 M, USA), making a gauge length of 600 mm. Tensile testing was performed using an Instron 5985 instrument (Instron, USA) at a loading speed of 2 mm/min with a 100 kN load cell. Bending testing was also performed with the specimens prepared according to ASTM D790 ($55 \times 12.7 \times 2$ mm). A universal tensile tester (Quasar 50, Galdabini, Italy) equipped with a three-point loading system was used for bending tests. The crosshead speed was 1.0 mm/min, and the sample span-to-depth ratio was 16:1. A minimum of five specimens were tested.

3. Results and discussion

3.1. Fabrication of 3D woven preforms and composites

3.1.1. Various 3D woven structures by different z-binder interlacing

To investigate the effect of different z-binder interlacings on the 3D woven structures, we fabricated three representative 3D woven preforms in a three-layer through-thickness structure (Fig. 3). All the three structures contained six wefts in a repeat cycle. As shown in Fig. 3 (a), the TTO structure contains z-binder yarns that wrap around three weft yarns covering the entire z-direction. The TTLL structure has z-binder yarns that wrap around one weft yarn and then two weft yarns (Fig. 3 (b)), whereas the TTAL structure has z-binder yarns that wrap each weft yarn, i.e., wrap three times, one at a time (Fig. 3(c)). These weaving structures were fabricated by adjusting the weaving process. To clarify explain this and in fact monitor the weaving process, a weaving process diagram is devised and given in Fig. 3(d)–(f). In the weaving process diagrams, the z-binder and warp heddles are represented by "B" and "W" and the numbers behind these denote different heddles that are used to achieve the desired weaving pattern. Note that the colors in the

Table 1
Specification of textile architecture of 3D woven composites.

Parameter	3D woven composite		
	TTO	TTLL	TTAL
Warp fiber count	6 K	6 K	6 K
Weft fiber count	12 k	12 k	12 k
z-binder fiber count	3 k	3 k	3 k
Warp density (ends/cm)	4	4	4
Weft density (picks/cm)	6	6.92	7.66
z-binder density (binders/cm)	4	4	4
Areal density (g/m^2)	747.4	910.3	1057.9
Composite thickness (mm)	1.71	1.98	2.19

Table 2
Volume fraction (%) of constituent (fiber, matrix, and void) in the 3D woven composites.

Constituent	3D woven composite		
	TTO	TTLL	TTAL
Fiber	51.06 ± 0.44	52.13 ± 0.36	53.33 ± 0.57
Matrix	47.00 ± 0.38	45.75 ± 0.33	44.39 ± 0.42
Voids	1.94 ± 0.04	2.12 ± 0.20	2.28 ± 0.74

diagram match the colors of warp, weft, and z-binder yarns in the 3D woven structures. The lifting and lowering of a specific heddle are indicated by the filled and blank sections of the diagram, respectively. The first weaving steps for all the three structures were identical. The initial weft was inserted and woven below the raised B1, W1, and W2 heddles and above the descended B2 heddle. As shown in Fig. 3(d), the second weft for the TTO structure was woven below the raised B1 and W1 heddles and above the descended B2 and W2 heddles. In contrast, the second wefts of the TTLL and TTAL structures were woven below the raised B2 and W1 heddles and above the descended B1 and W2 heddles, as shown in Fig. 3(e) and (f). For the third weft, the B1 heddle was raised in the TTO and TTAL structure, whereas the B2 heddle was raised in the TTLL structure. Although W1 and W2 were the same configuration for all three structures, different motions of B1 and B2 heddles wrapped wefts by the z-binders simultaneously, fabricating the desired pattern and structure.

Fig. 4 shows 3D geometrical solid models of the three representative 3D woven structures discussed above and real CT images of their fabricated 3D woven composites manufactured using our proposed weaving mechanism. After cutting the samples into dimensions of x = 30 mm and y = 5 mm, micro-CT scanning, reconstruction, and volume rendering were performed sequentially. The micro-CT results were in agreement with the designed structures, indicating that the weaving process was successful. Upon closer examination of each structure, as shown in Fig. 4(a) and (d) (and (g) and (j)), the TTO structure exhibited densely arranged wefts in the z-direction because of the z-binders surrounding the three wefts. Conversely, in the TTAL structure, as shown in Fig. 4(c) and (f) (and (i) and (l)), the z-binders were wrapped around each weft, resulting in regularly spaced wefts. As shown in Fig. 4(b) and (e) (and (h) and (k)), the TTLL structure was an intermediate form between the TTO and TTAL structures, i.e., the z-binder wrapped one and two wefts in subsequent cycle. As such, the weft yarns were not evenly arranged and were slightly twisted.

3.1.2. Effect of z-binder interlacing on directional fiber volume fraction

The three structures (TTO, TTLL, and TTAL) exhibit different z-binder waviness and patterns, which significantly influence the textile architecture of 3D woven composites [18,19,22]. The specification of textile architecture of the fabricated 3D woven composites are listed in Table 1. The warp, weft, and z-binder fibers had counts of 6K, 12K, and 3K, respectively. The numbers of yarns per unit length for the warp, weft, and z-binder are listed in the table as ends/cm, picks/cm, and binders/cm, respectively. The areal density of the dry 3D woven preform, measured in g/m^2, and the thickness of the 3D woven composite (measured in mm) are also provided in the table. Because of the large curvature of the z-binder yarn of TTAL structure, which interlaces all wefts, a thinner yarn than the warp or weft was selected for the z-binder. The z-binder architecture significantly affects void content, directional fiber volume fraction, mechanical properties, failure mechanisms, and other factors [22]. All the warp densities were the same, whereas the weft density and thickness varied depending on the z-binder architecture. The weft and z-binder densities vary due to these structural differences. Notably, the warp density for all these structures remains constant at 4 ends/cm. However, the weft density increases progressively from 6, 6.92 to 7.66 picks/cm, respectively. Initially, the z-binder density is uniform at 4 binders/cm across all structures, but it subsequently increases to 5.37, 9.82, and 14.24 binders/cm, respectively, based on the specific structure. Consequently, the area density increases from TTO to TTAL. In the micro-CT image presented in Fig. 4, the weft yarn in the TTO structure is a long oval shape in the x-direction. Conversely, in the TTAL structure, the weft yarn closely approaches a circular shape due to the wrapping of all weft yarns by the z-binder. This z-binder influence leads to an increase in the thickness of the structure, particularly in the case of the TTAL structure.

Table 2 lists the fiber, matrix, and void volume fractions of the 3D woven composites. The TTAL structure exhibited the highest fiber volume fraction (53.33 %), which is attributed to its high z-binder content. However, it also had the highest void content of 2.28 % because the z-binders induced more voids in the 3D woven composites than in the 2D composites [59,60]. The z-binders reduced the

Table 3
Directional fiber volume fraction (%) of the 3D woven composites.

Direction of yarn	3D woven composite		
	TTO	TTLL	TTAL
Warp	10.93	9.16	8.07
Weft	32.79	31.72	30.91
z-binder	7.34	11.25	14.35

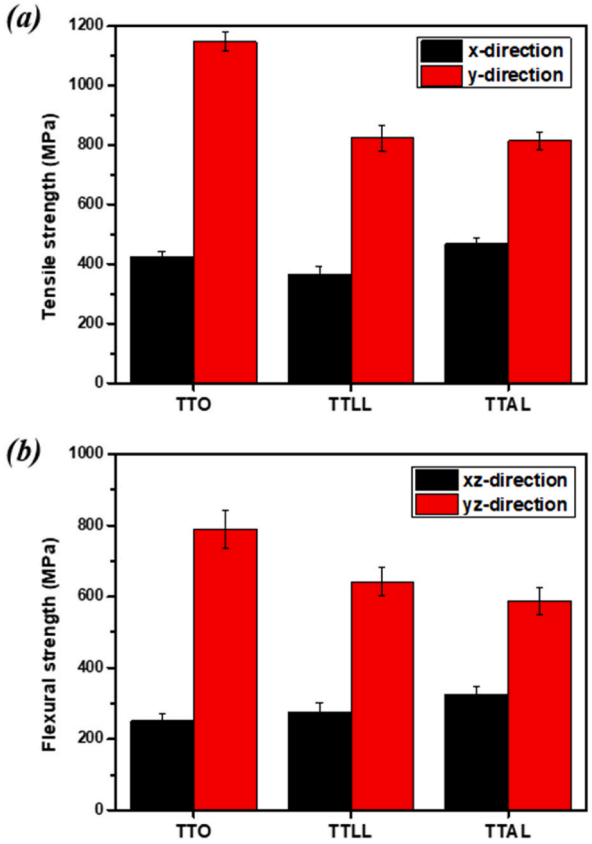

Fig. 5. (a) Tensile strength of the three 3D woven composites measured in x- and y-directions and (b) their flexural strength measured in xz- and yz-directions.

resin flow between the warp and weft yarns, thereby decreasing the amount of resin in the area. The TTLL structure had a smoother (i.e., small curvature of z-binder yarn) weaving pattern than the TTAL structure, whereas the TTO structure had the smoothest pattern. A smoother weaving pattern results in a better resin flow between the woven layers and resin infiltration into the woven fabric [22], which leads to a lower void content. Thus, the TTO structure had the lowest void content, and the TTAL structure had the highest void content with the most complex weaving pattern.

The directional fiber volume fractions, which were obtained by the total fiber volume fraction with the warp, weft, and z-binder contents, are listed in Table 3. From TTO to TTAL structures, the wrapping region of the z-binder yarns around the weft yarns was increased. This alteration created more space between the warp layers in the composites, leading to larger dimension in the xz-plane. Despite having the same number of warp yarns, the increased dimensions resulted in a reduced fiber volume fraction. As a result, the TTAL structures exhibited the lowest fiber volume fraction in the warp direction. Conversely, the expansion of the wrapping region of the z-binder yarn led to a higher fiber volume fraction in the z-binder direction. This is evident from the TTAL structure, which showed the highest fiber volume fraction in the direction. It is important to note that while the majority of z-binder yarns in the TTO structure were aligned with the thickness direction, in the other two cases, some sections of the z-binder yarns were not aligned. Taking into account the influence of the z-binder on the x- and z-directions, we calculated the fiber volume fraction in the x-, y-, and z-directions. The values are listed in Table S1. The TTAL structure exhibited higher x- and z-direction fiber volume fractions compared to the other two structures, owing to the high z-binder fiber volume fraction. Considering the overall thin structure and the significant curvature of the z-binder in the TTAL structure, the fiber volume fraction in the z-direction was relatively low. However, this can be further

increased by adjusting the structure's thickness and a different type of yarn, making it possible to fabricate full 3D woven preform. Subsequently, the mechanical properties of the three 3D woven composites were investigated as follows.

3.1.3. Mechanical properties of 3D woven composites

The mechanical properties of composite materials are mainly influenced by the fiber orientation and fiber volume fraction. According to previous studies, yarn waviness has a significant negative effect on the properties of 3D woven composites [19,61]. Because the TTO, TTLL, and TTAL structures are all based on the TT structure, the yarn waviness is generally large and similar; therefore, the mechanical properties were mainly affected by the total and directional fiber volume fractions.

The tensile strengths in the x- and y-directions for all the samples are shown in Fig. 5(a). The reason why the tensile strength in the y-direction was greater than that in the x-direction was that weft was 12k, which had a higher fiber count than warp (6K), and the directional fiber volume fraction of the weft was high. The tensile strength of the used weft yarn was 4200 MPa. Therefore, for the three structures in which the volume fraction of weft was about 30 %, the y-direction tensile strength can be predicted to be approximately 1260 MPa. The TTO structure exhibited the largest y-directional tensile strength (1146.6 MPa), which can be attributed to the low z-binder content and the resulting high directional fiber volume fraction of the weft. In contrast, the TTAL structure had a small y-direction tensile strength (813.6 MPa) owing to the decrease in the weft directional fiber volume fraction caused by the z-binder interlacing all wefts at regular intervals, as well as the increased void content owing to the complex z-binder pattern and thicker structure.

The reason why the tensile strength in the x-direction was smaller than that in the y-direction was because the warp was set at 6k and a fiber count lower than that of the weft (12K) was used, and the directional fiber volume fraction of the warp is low. The tensile strength of the used warp yarn is 3800 MPa. Therefore, for the three structures in which the volume fraction of weft is about 10 %, the x-direction tensile strength can be predicted to be approximately 380 MPa. However, the z-binder was continuously supplied and arranged in the xz-plane, which had the effect of increasing the directional fiber volume fraction in the x-direction and the z-direction. The z-binder directional fiber volume fractions of TTO, TTLL, and TTAL structures were 7.34 %, 11.25 %, and 14.35 %, respectively (Table 3). Considering the z-binder's influence on the x-direction, each structure augmented the fiber volume fraction in this direction by 5.47 %, 9.16 %, and 12.10 %. Despite TTAL having the lowest fiber volume fraction in the warp direction, the substantial z-binder content (i.e., higher fiber volume in the x-direction) led to the largest tensile strength (467.9 MPa) in the x-direction for the TTAL structure. On the other hand, the fiber volume fraction in the warp direction was the highest in the TTO structure, but such a low z-binder content (i.e., lower fiber volume in the x-direction) resulted in a smaller tensile strength (423.2 MPa) of the TTO structure in the x-direction. The TTLL structure was considered an intermediate form between the TTO and TTAL structures, with the number of z-binder interlacing wefts repeating one and two. Owing to this non-uniform structure, the TTLL structure tended to be slightly twisted and had a smaller tensile strength in both the x-direction (365.5 MPa) and y-direction (823.7 MPa).

The flexural strengths in the xz- and yz-directions for all samples are shown in Fig. 5(b). Similar to the previous tensile strength results, the flexural strength in the yz-direction was greater than that in the xz-direction owing to the high directional fiber volume fraction of the weft direction. The most influential factor affecting flexural strength in this direction is the directional fiber volume fraction of the weft. Specifically, the weft's directional fiber volume fractions for the TTO, TTLL, and TTAL structures were 32.79 %, 31.72 %, and 30.91 %, respectively (refer to Table 3). Similar to the tensile strength results, the TTO structure had the largest yz-direction flexural strength (788.7 MPa), whereas the TTAL structure had the smallest flexural strength (587.1 MPa).

Conversely, the TTAL structure demonstrated the highest flexural strength in the xz-direction. In this case, the primary influencing factor is the fiber volume fraction in both the x- and z-directions. The TTAL structure's x-direction and z-direction fiber volume fractions were 20.17 % and 2.25 %, respectively, which surpass those of the TTO and TTLL structures (see Table S1). As a result, in the xz-direction, the TTAL structure exhibited the highest flexural strength (325.5 MPa). On the contrary, the TTO structure, which possesses the lowest directional fiber volume fraction in the x- and z-directions, displayed the lowest flexural strength (250.6 MPa).

Considering the thickness direction of the z-binder, the TTO, TTLL, and TTAL structures have the effect of increasing the fiber volume fraction in the thickness direction by 1.87 %, 2.09 %, and 2.25 %, respectively. An increase in the z-binder content improved both the x-direction tensile strength and the xz-direction flexural strength. The high z-binder content (i.e., higher fiber volume in the thickness direction) resulted in the largest flexural strength (325.5 MPa) of the TTAL structure in the xz-direction. On the other hand, the low z-binder content (i.e. lower fiber volume in the thickness direction) resulted in the smallest flexural strength (250.6 MPa) of the TTO structure in the xz-direction.

The advantage of the structures we presented is that we observed differences in the mechanical properties of the structures based on the degree of interlacing of the z-binder. The TTAL structure exhibits a very high z-binder fiber volume fraction of 14.35 %, ensuring continuity in the xz-direction throughout the structure and thereby enhancing mechanical properties in both the x- and z-directions. Previous studies consistently reported larger mechanical properties in the y-direction [21,22]. Therefore, the significant improvement in mechanical properties in the x- and z-directions, which initially had relatively smaller values, is noteworthy.

3.2. Fabrication of seamless 3D woven preforms with complex shape

Utilizing the aforementioned weaving processes in section 3.1.1, various 3D woven preforms with variable heights in the thickness can be fabricated by devising a new weaving process. The TTAL structure encompasses all the weft yarns, thereby allowing for the production of a wider range of structures with modifications. We can control the amount of yarns used during the weaving process and ensure consistent length movement throughout by employing tension control and pitch shift. Through precise control of the weaving process, we can successfully weave TTAL structures even with significant waviness (see Fig. 2). As depicted in Fig. 4, the TTAL

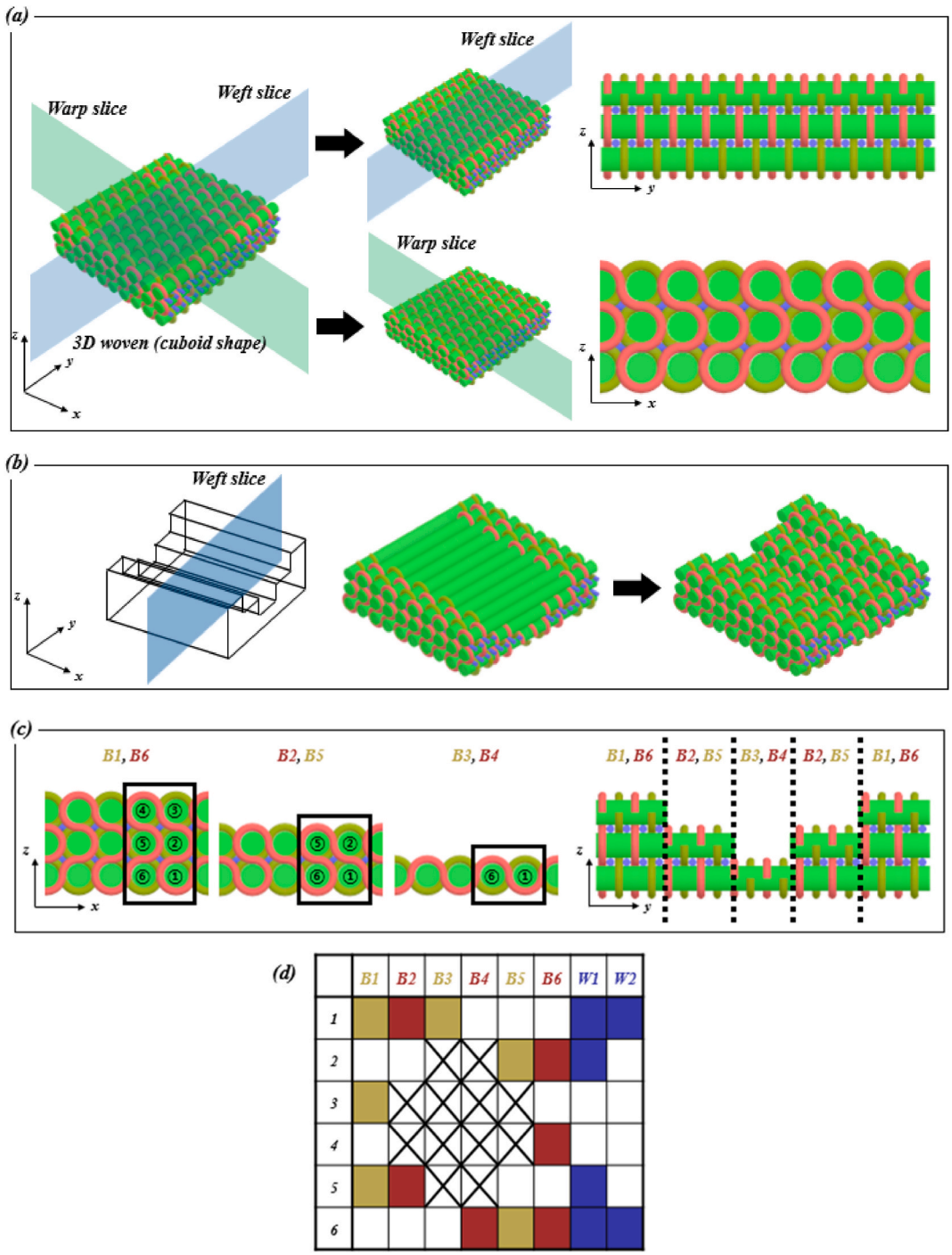

Fig. 6. (a) Manufacturing of 3D complex woven preforms using the concept of weft and warp slices, (b) concave 3D woven structures manufactured through weaving process setting and post-processing. (c) 2D plane view model of a concave structure with different heights fabricated by selective wrapping of z-binder yarns: B1, B6 (3-layer part), B2, B5 (2-layer part), B3, B4 (1-layer part). (d) Weaving process diagram of concave 3D woven structures.

structure boasts geometric consistency, as all wefts maintain a uniform circular shape due to the z-binder yarns surrounding them. This represents a distinct structural advantage, particularly when creating complex shapes with increasing layers.

As illustrated in Fig. 6(a), weft and warp slices [48] can be incorporated into a 3D woven preform. Here, a 'slice' denotes a cross-section in a specified direction, while a 'weft slice' refers to a fiber arrangement on a cross-section along the weft direction (or a cross-section perpendicular to the warp direction). By consistently considering the desired cross-sectional shape of the woven preform

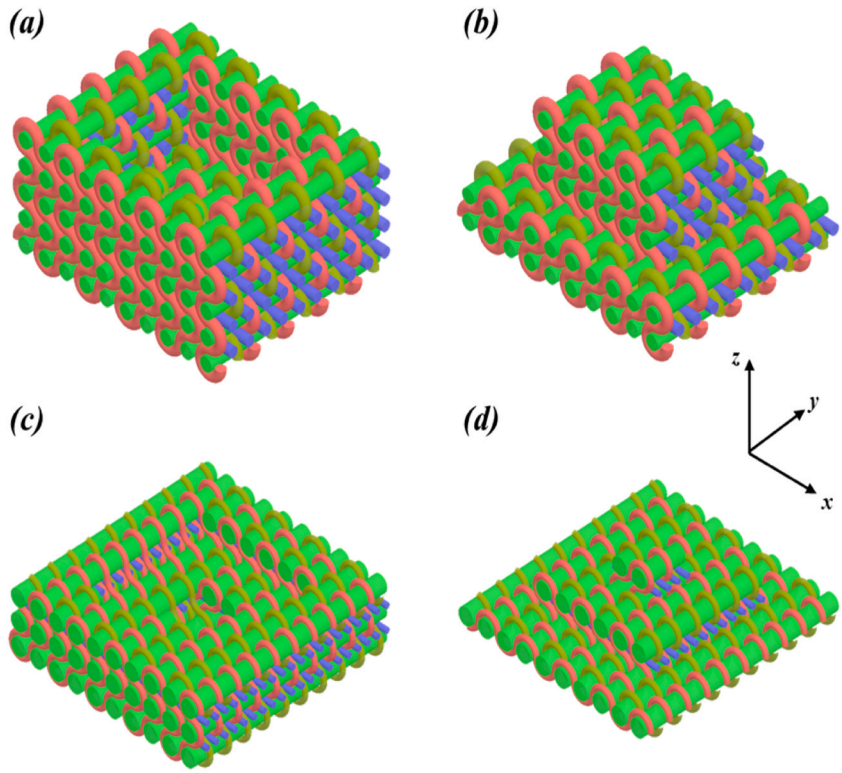

Fig. 7. Seamless and further complex 3D woven structures: (a) box-, (b) box lid-, (c) bowl-, and (d) pyramid-shaped 3D woven structures.

and thereby designing the weaving process, various non-uniform structures can be achieved during the preform stage. The three 3D woven structures (TTO, TTLL, and TTAL) produced in this study have a cuboid shape with uniform height in the z-direction. At this configuration, both the weft slice (yz-plane cross-section) and warp slice (xz-plane cross-section) are rectangular. However, as the structure evolves into a more complex shape, there may be instances where the weft and warp slices are not rectangular. Fig. 6(b) provides an example of a specific 3D shape with an introduced weft slice. Subsequently, a new 3D weaving method is elucidated to fabricate this particular 3D shape. By continuously considering the desired cross-sectional shape of the woven preform and thus designing a weaving process, the target structure can be obtained during the preform stage. Taking a weft slice as an example, this new 3D weaving concept will be explained as follows.

3.2.1. Weaving of 3D woven preform with a concave cross-section

The fundamental and original concept behind creating a 3D woven preform with a concave shape at its center involves the utilization of z-binder yarns. This is achieved by intentionally omitting the wrapping of z-binder yarns around the weft yarns in a selective manner. During the weaving process, both the warp and weft yarns intervene through all parts of the preform, whereas the z-binder involves only with the necessary parts, preventing unnecessary parts from being woven. The warp and weft in areas without the z-binder is cut out in post-processing. Using this method, continuous and seamless 3D complex woven preforms can be manufactured (see Fig. 6(b) for a schematic illustration of concave 3D woven preform that can be fabricated as an example).

The TTAL structure is used as a basis for weaving concave-shaped 3D woven preform. Fig. 6(c) shows the 2D plane view model of a concave structure with different heights. 6 z-binder yarns are used; B1, B6 (3-layer part), B2, B5 (2-layer part), and B3, B4 (1-layer part) created a concave structure with a layer number of 3-2-1-2-3 in x and z plane (we denote this structure by "concave <3−2−1−2−3>"). For the 3-layer, B1 and B6 are not omitted in the weaving process, while two weaving processes are omitted in B2 and B5, forming the 2-layer. Lastly four weaving processes are omitted in B3 and B4 for the 1-layer. A weaving process diagram of this structure is presented in Fig. 6(d). The omission of the z-binder in the weaving process is denoted by 'X' mark because the concave structure exhibits a partial deficiency compared to the TTAL structure. In the aspect of the descent of the heddle, the unmarked and X-marked sections represent the identical movement; however, the X-marked sections highlight the omission of the corresponding processes, making it easier to identify areas where the z-direction height difference occurs, and more intuitive to understand the height difference in the z-direction. Then, a concave <3−2−1−2−3> 3D woven preform was manufactured using this weaving setup. The unnecessary warp and weft of the inner part without the z-binder were removed through a step-by-step post-processing procedure after weaving. Subsequently, a concave 3D woven preform was obtained, as shown in Fig. S1, with a 3-layer (red) section on the outside, a 2-layer (orange) sections on the sides, and a 1-layer (yellow) section in the center.

Similarly, a convex 3D woven structures with a layer number of 1-2-3-2-1 in x and z plane (i.e., convex <1−2−3−2−1>) can be

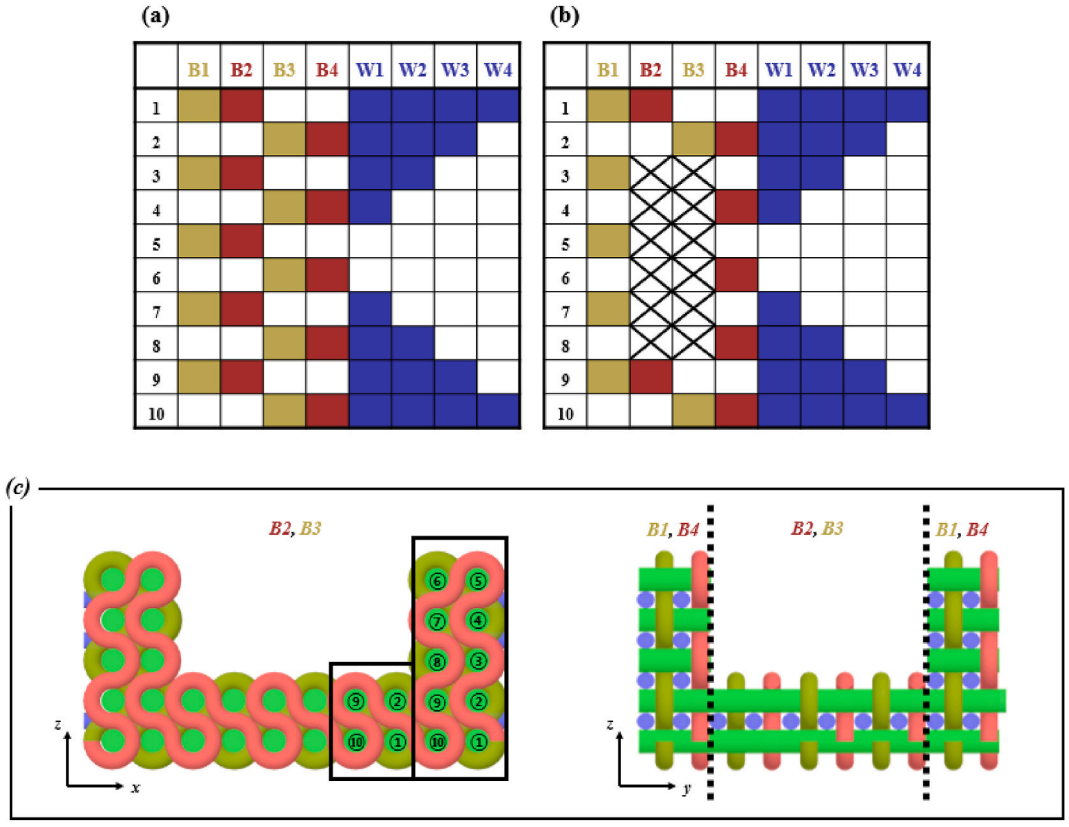

Fig. 8. Weaving process diagram of a 3D box-shaped woven preform using weft slice (concave <5−2−5>) and warp slice (concave <5−2−5>): (a) 5-layer part, (b) 2-layer part. (c) 2D plane view model of a 3D box structure with different heights fabricated by selective wrapping of z-binder yarns: B1, B4 (5-layer part), B2, B3 (2-layer part).

fabricated using the same manner as that for the concave 3D woven structure (see Fig. S2). A convex <1−2−3−2−1> 3D woven preform was manufactured using the weaving process setup. The unnecessary warp and weft of the outer part without the z-binder were removed through a step-by-step post-processing procedure after weaving. Subsequently, a convex 3D woven preform was obtained, as shown in Fig. S3, with a 3-layer (red) section at the center, a 2-layer (orange) sections on the sides, and a 1-layer (yellow) section on the outside.

3.2.2. Manufacturing of seamless and complex 3D woven preforms and their composites

A weaving process was established for both concave and convex 3D woven structures using only weft slices. Moreover, by incorporating both weft and warp slices, 3D woven preforms with even greater complexities can be manufactured. By following the established weaving mechanism in section 3.2.1, it is possible to seamlessly create complex structures such as boxes (Fig. 7(a)), box lids (Fig. 7(b)), bowls (Fig. 7(c)), and pyramids (Fig. 7(d)), all of which have non-uniform heights along the z-axis. Each structure can be denoted as a combination of weft and warp slices, e.g., box type of seamless 3D woven preform can be manufactured by a combination of concave <5−2−5> for weft slice and concave <5−2−5> for warp slice. Similarly, other three structure in Fig. 7 can be fabricated by a combination of these slices; box lid (convex <2−5−2> + convex <2−5−2>), bowl (concave <3−2−1−2−3> + concave <3−2−1−2−3>), and pyramid (convex <1−2−3−2−1> + convex <1−2−3−2−1>).

When producing complex 3D woven structures, a weaving process should be considered depending on both the weft and warp slices. Although using only the weft slice allows the entire structure to be manufactured with one weaving process setting, incorporating the warp slice requires changing the weaving process setting whenever there is a change in the height in the x-direction. This means that, to manufacture more complex shapes, multiple weaving processes must be set up and subsequently carried out. To demonstrate the capability of the current weaving method to manufacture complex-shaped 3D woven structures, a weaving process was set up for a 3D box structure using both weft slice (concave <5−2−5>) and warp slice (concave <5−2−5>). As the number of layers increased to 5, there were two more warp heddles than in the 3-layer structure. The weaving process for the two parts had 10 steps per cycle; however, as shown in Fig. 8, the degree of omission in the weaving process was different. As shown in Fig. 8(a), the outer 5-layer has the same weaving process pattern as the previous TTAL structure but with an increased number of z-binder heddles and warp heddles. As shown in Fig. 8(b), in the central 2-layer part, six weaving processes were omitted in the z-binder heddles B2 and B3. Compared with the box lid weaving process, only the order of the z-binder heddles changed. In the subsequent weaving process, it

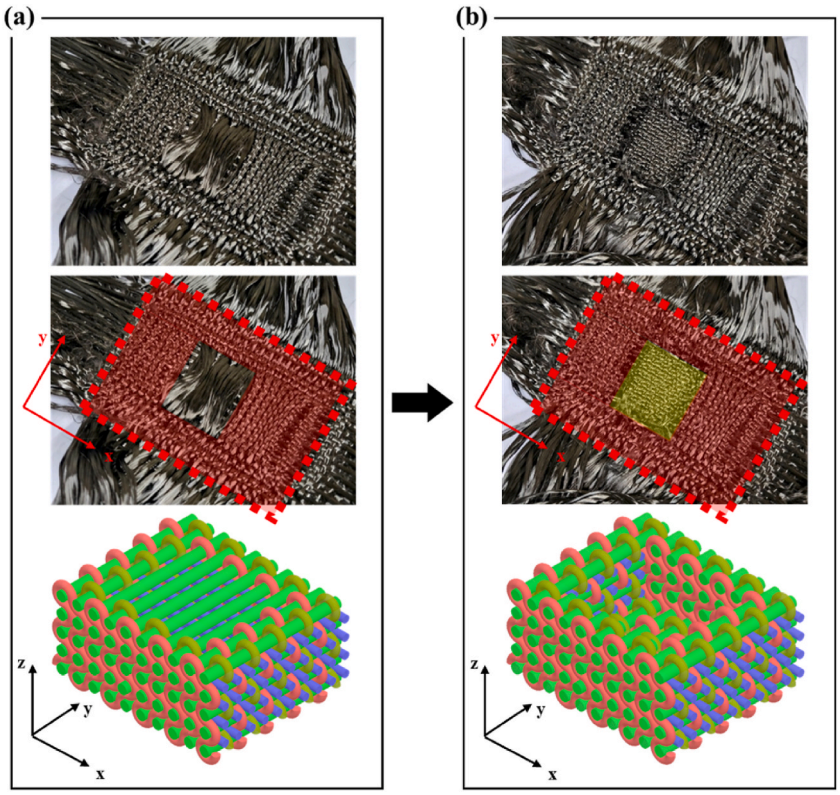

Fig. 9. A 3D box-shaped woven preform fabricated using weft slice (concave <5−2−5>) and warp slice (concave <5−2−5>): (a) 5-layer part for box wall and (b) 2-layer part for box bottom.

can be predicted that only the center of the structure will have a lower height, as indicated by the X mark. Fig. 8(c) shows the 2D plane view model of a 3D box structure with different heights fabricated by selective wrapping of z-binder yarns: B1, B4 (5-layer part), B2, B3 (2-layer part) created a 3D box structure.

A 3D box-shaped woven preform was manufactured using the weaving process setup above. After weaving, as shown in Fig. 9(a), the unnecessary warp and weft of the inner part without the z-binder were cut from above using a step-by-step post-processing process. A 3D box-shaped woven preform was obtained, as shown in Fig. 9(b), with a low height only in the center of the structure, a 5-layer (red) section on the outside and a 2-layer (yellow) section in the center. Next, 3D composites were manufactured using resin transfer molding. Fig. 10(a) shows the manufactured seamless 3D box-shaped woven composite. A micro-CT scan analysis was performed to observe the fiber structure of the composites. It can be confirmed that the 3D woven composite (Fig. 10(c)) was manufactured consistently with the designed structure (Fig. 10(b)), indicating that the weaving process was successful. In addition, the micro-CT scan revealed that the z-binders continuously wrapped the weft at the boundary, where the height difference occurred in the xz-plane cross-section. The structure was seamless with continuity in the xz-direction. This confirmed the continuity of the complex-shaped seamless 3D woven structure.

The weaving structure depicted in Fig. 7 presents an economic disadvantage due to the necessity of cutting unnecessary warp and weft yarns in the post-processing stage. However, considering the final shape, the presence of continuity of z-binder yarns throughout the structure is evident, which constitute a substance advantage in terms of mechanical integrity. Although mechanical testing was not conducted for the complex shape, the continuity within the structure was confirmed through micro-CT results (Fig. 10). As the structure becomes more complex, the gap in continuity will likely increase. Therefore, our method holds significant advantages for more complex structures at larger scales.

3.2.3. Further examples of seamless 3D complex woven preforms

By utilizing both weft and warp slices, we set up a weaving process for the box lid structures (Figs. S4 and S5), which had a large height difference between the components, and successfully manufactured 3D woven preforms. Owing to the continuous weaving and post-processing processes, the z-binder maintained its continuity even when the height difference was significant. Bowl and pyramid structures may also be designed and manufactured with three gradual height differences, as shown subsequently. As the degree of complexity increased, a succession of three weaving processes was necessary to create the desired structure (Figs. S6 and S7 for bowl structure and Figs. S8 and S9 for pyramid structure). More discussion on these preform design and weaving can be found in supplementary information. Then, resin was transferred to manufacture the composite from these 3D woven preform (Fig. S10). We

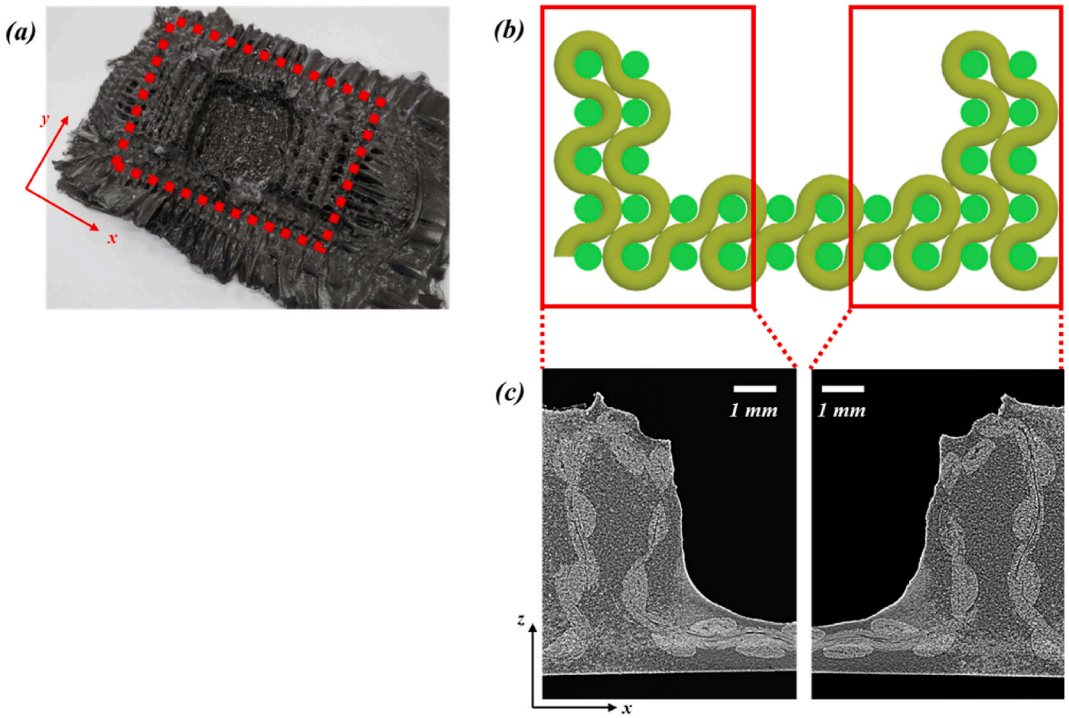

Fig. 10. (a) Seamless 3D box-shaped woven composite, (b) designed structure, and (c) actual observations of the xz-plane cross-section of the composite.

successfully developed a mechanism that enables the manufacturing of 3D woven structures for any combination of weft and warp slices in various complex shapes. The possibilities are endless, as long as the equipment can handle the increased complexity of the weaving process. Seamless 3D boxes, box lids, bowls, and pyramid-shaped woven preforms have numerous potential applications in various industries. The weaving method discussed in the manuscript can be applied to manufacture 3D box shapes of increasing complexity, including cylinder-shaped 3D woven structures and box-in-box 3D woven structures (Fig. S11). These structures have potential applications in various fields, such as battery packs, containers, or continuously repeated lattice structures. Consequently, our weaving method offers significant advantages in terms of structural design, seamlessness, continuity, structural integrity, and mechanical properties.

4. Conclusion

Three representative 3D woven structures were manufactured according to the degree of z-binder interlacing using a new weaving mechanism with a 3D weaving equipment. The directional fiber volume fraction, tensile strengths, and flexural strengths of each structure were characterized. The TTAL structure had a higher z-binder fiber volume fraction, resulting in greater tensile strength and flexural strength in the x- and xz-direction, respectively, owing to the increased complex directional fiber volume fraction. Using this weaving mechanism, a process for manufacturing seamless 3D complex woven preforms with concave and convex shapes of nonuniform heights in the z-direction was developed. As demonstrated, this process enables the manufacture of complex shapes such as boxes, box lids, bowls, and pyramid-shaped preforms. The micro-CT analysis confirmed the continuity of the complex shapes of the resulting 3D woven composites. This weaving mechanism has great potential for the development of even more complex and diverse structures, which can overcome the various disadvantages of composite materials and find applications in various industrial fields.

Ethical approval

Not applicable.

Data availability

The raw/processed data required to reproduce these findings cannot be shared at this time due to legal or ethical reasons.

CRediT authorship contribution statement

Hyun Joon Yang: Conceptualization, Methodology, Writing - original draft, Writing - review & editing. **Doyoung Kim:** Data curation, Investigation. **Kyeong Mo Kang:** Validation, Visualization. **Woong-Ryeol Yu:** Supervision, Writing - review & editing.

Declaration of competing interest

The authors declare that they have no known competing financial interests or personal relationships that could have appeared to influence the work reported in this paper.

Acknowledgement

This work was supported by the National Research Foundation of Korea (NRF) grant funded by the Korea government (MSIT) (No. 2023R1A2C2006014).

Appendix A. Supplementary data

Supplementary data to this article can be found online at https://doi.org/10.1016/j.heliyon.2024.e24121.

References

[1] N. Odagiri, H. Kishi, M. Yamashita, Development of TORAYCA prepreg P2302 carbon fiber reinforced plastic for aircraft primary structural materials, Adv. Compos. Mater. 5 (3) (1996) 249–254.
[2] J. Park, et al., Electromechanical modeling of unidirectional CFRP composites under tensile loading condition, Compos. Appl. Sci. Manuf. 33 (2) (2002) 267–275.
[3] J.B. Park, T. Okabe, N. Takeda, New concept for modeling the electromechanical behavior of unidirectional carbon-fiber-reinforced plastic under tensile loading, Smart Mater. Struct. 12 (1) (2003) 105.
[4] F. Shen, K. Lee, T. Tay, Modeling delamination growth in laminated composites, Compos. Sci. Technol. 61 (9) (2001) 1239–1251.
[5] V.P. Nguyen, P. Kerfriden, S.P. Bordas, Two-and three-dimensional isogeometric cohesive elements for composite delamination analysis, Compos. B Eng. 60 (2014) 193–212.
[6] D.D. Cartie, et al., 3D reinforcement of stiffener-to-skin T-joints by Z-pinning and tufting, Eng. Fract. Mech. 73 (16) (2006) 2532–2540.
[7] I.K. Partridge, D.D. Cartié, Delamination resistant laminates by Z-Fiber® pinning: Part I manufacture and fracture performance, Compos. Appl. Sci. Manuf. 36 (1) (2005) 55–64.
[8] A. Mouritz, Review of z-pinned composite laminates, Compos. Appl. Sci. Manuf. 38 (12) (2007) 2383–2397.
[9] K. Dransfield, C. Baillie, Y.-W. Mai, Improving the delamination resistance of CFRP by stitching—a review, Compos. Sci. Technol. 50 (3) (1994) 305–317.
[10] A. Mouritz, B. Cox, A mechanistic interpretation of the comparative in-plane mechanical properties of 3D woven, stitched and pinned composites, Compos. Appl. Sci. Manuf. 41 (6) (2010) 709–728.
[11] J.-H. Byun, et al., Impact properties of laminated composites with stitching fibers, Compos. Struct. 76 (1–2) (2006) 21–27.
[12] G. Dell'Anno, J. Treiber, I.K. Partridge, Manufacturing of composite parts reinforced through-thickness by tufting, Robot. Comput. Integrated Manuf. 37 (2016) 262–272.
[13] R. Sadeghian, et al., Manufacturing carbon nanofibers toughened polyester/glass fiber composites using vacuum assisted resin transfer molding for enhancing the mode-I delamination resistance, Compos. Appl. Sci. Manuf. 37 (10) (2006) 1787–1795.
[14] Y. Li, Y.-W. Mai, L. Ye, Effects of fibre surface treatment on fracture-mechanical properties of sisal-fibre composites, Compos. Interfac. 12 (1–2) (2005) 141–163.
[15] H. Yang, et al., Continuous and rapid production of three-dimensional woven fabric preforms using a new weaving technique, Functional Composites and Structures 2 (1) (2020) 15005.
[16] N. Gokarneshan, R. Alagirusamy, Weaving of 3D fabrics: a critical appreciation of the developments, Textil. Prog. 41 (1) (2009) 1–58.
[17] O.A. Golra, et al., Strategy for introducing 3D fiber reinforced composites weaving technology, Procedia Technology 1 (2012) 211–216.
[18] Y. Liu, et al., Research on development of 3D woven textile-reinforced composites and their flexural behavior, Mater. Des. 212 (2021) 110267.
[19] Q. Hu, et al., A comprehensive study on the mechanical properties of different 3D woven carbon fiber-epoxy composites, Materials 13 (12) (2020) 2765.
[20] K. Bilisik, et al., Three-dimensional fully interlaced woven preforms for composites, Textil. Res. J. 83 (19) (2013) 2060–2084.
[21] M.N. Saleh, C. Soutis, Recent advancements in mechanical characterisation of 3D woven composites, Mechanics of Advanced Materials and Modern Processes 3 (1) (2017) 1–17.
[22] M.N. Saleh, et al., Characterising the loading direction sensitivity of 3D woven composites: effect of z-binder architecture, Compos. Appl. Sci. Manuf. 90 (2016) 577–588.
[23] T. Huang, Y. Wang, G. Wang, Review of the mechanical properties of a 3D woven composite and its applications, Polym.-Plast. Technol. Eng. 57 (8) (2018) 740–756.
[24] Y. Liu, H. Xia, Q.-Q. Ni, Experimental investigation on low-velocity impact performance of 3D woven textile composites, Appl. Compos. Mater. 29 (1) (2022) 121–146.
[25] H. Lansiaux, et al., Development and multiscale characterization of 3D warp interlock flax fabrics with different woven architectures for composite applications, Fibers 8 (2) (2020) 15.
[26] Y.S. Perera, et al., Evolution of 3D weaving and 3D woven fabric structures, Fashion and Textiles 8 (1) (2021) 1–31.
[27] S. Weerasinghe, et al., Method and apparatus to weave a fully interlaced three-dimensional textile structure, in: 2017 Moratuwa Engineering Research Conference (MERCon), IEEE, 2017.
[28] M.I. Khan, et al., Development of composites, reinforced by novel 3D woven orthogonal fabrics with enhanced auxeticity, J. Ind. Textil. 49 (5) (2019) 676–690.
[29] R. Kamiya, et al., Some recent advances in the fabrication and design of three-dimensional textile preforms: a review, Compos. Sci. Technol. 60 (1) (2000) 33–47.
[30] X. Chen, Advances in 3D Textiles, Elsevier, 2015.
[31] X. Chen, L.W. Taylor, L.-J. Tsai, An overview on fabrication of three-dimensional woven textile preforms for composites, Textil. Res. J. 81 (9) (2011) 932–944.
[32] A. Hao, et al., Dynamic properties of 3-D orthogonal woven composite T-beam under transverse impact, Compos. Appl. Sci. Manuf. 39 (7) (2008) 1073–1082.
[33] C. Ji, et al., Impact damage of 3D orthogonal woven composite circular plates, Appl. Compos. Mater. 14 (2007) 343–362.

[34] Y. Luo, et al., Transverse impact behavior and energy absorption of three-dimensional orthogonal hybrid woven composites, Compos. Struct. 81 (2) (2007) 202–209.
[35] L. Yan, N. Chouw, K. Jayaraman, Flax fibre and its composites–A review, Compos. B Eng. 56 (2014) 296–317.
[36] R. Gerlach, et al., In-plane and through-thickness properties, failure modes, damage and delamination in 3D woven carbon fibre composites subjected to impact loading, Compos. Sci. Technol. 72 (3) (2012) 397–411.
[37] A. Fuchs, et al., Laser cutting of carbon fiber fabrics, Phys. Procedia 41 (2013) 372–380.
[38] H. Saito, I. Kimpara, Evaluation of impact damage mechanism of multi-axial stitched CFRP laminate, Compos. Appl. Sci. Manuf. 37 (12) (2006) 2226–2235.
[39] M.R. Abusrea, et al., Bending strength of CFRP laminated adhesive joints fabricated by vacuum-assisted resin transfer molding, Compos. B Eng. 156 (2019) 8–16.
[40] N. Athanasopoulos, G. Sotiriadis, V. Kostopoulos, A study on the effect of Joule-heating during the liquid composite molding (LCM) process and on the curing of CFRP composite laminates 32 (2010) 11–15.
[41] M. Abusrea, et al., Strength enhancement of CFRP joints composed of partially unmolded laminates manufactured using Vacuum-Assisted Resin Transfer Molding (VARTM), J. Adhes. 99 (3) (2023) 379–405.
[42] A. Asadi, et al., A comparison of CFRP composite laminated joints fabricated with vacuum assisted resin transfer molding, Express Polym. Lett. 12 (9) (2018) 781–789.
[43] S. Yan, X. Zeng, A. Long, Experimental assessment of the mechanical behaviour of 3D woven composite T-joints, Compos. B Eng. 154 (2018) 108–113.
[44] C. Wu, et al., Influences of in-plane and out-of-plane fiber waviness on mechanical properties of carbon fiber composite laminate, J. Reinforc. Plast. Compos. 37 (13) (2018) 877–891.
[45] M. Thor, M.G. Sause, R.M. Hinterhölzl, Mechanisms of origin and classification of out-of-plane fiber waviness in composite materials—a review, Journal of Composites Science 4 (3) (2020) 130.
[46] P. Wang, et al., Experimental and numerical analyses of manufacturing process of a composite square box part: comparison between textile reinforcement forming and surface 3D weaving, Compos. B Eng. 78 (2015) 26–34.
[47] P. Wang, X. Legrand, D. Soulat, Investigation about the manufacturing technique of the composite corner fitting part, Autex Res. J. 14 (2) (2014) 111–120.
[48] R. Wu, et al., Automatic structure synthesis for 3D woven relief. ACM Transactions on Graphics (TOG) 39 (4) (2020) 102, 1-102: 10.
[49] P. Schegner, et al., Technology development for direct weaving of complex 3D nodal structures, Appl. Compos. Mater. 26 (1) (2019) 423–432.
[50] S. Lu, et al., Design and manufacture of 3D rectangular box-shaped fabrics, J. Ind. Textil. 47 (6) (2018) 1212–1225.
[51] A. Sayem, W. Kennon, N. Clarke, Int. J. Cloth. Sci. Technol. 22 (11) (2011).
[52] B.K. Behera, Z. Kamble, Advanced 3D woven profile structures and their composites for automotive applications, Polym. Compos. 43 (9) (2022) 5946–5953.
[53] K. Layng, et al., Cave: making collective virtual narrative, in: ACM SIGGRAPH 2019 Art Gallery, 2019, pp. 1–8.
[54] S. Bhattacharya, M. Koranne, Novel method of weaving three-dimensional shapes, Int. J. Cloth. Sci. Technol. 24 (1) (2012) 56–63.
[55] S. Rudov-Clark, et al., Fibre damage in the manufacture of advanced three-dimensional woven composites, Compos. Appl. Sci. Manuf. 34 (10) (2003) 963–970.
[56] M.A. Abtew, et al., Yarn degradation during weaving process and its effect on the mechanical behaviours of 3D warp interlock p-aramid fabric for industrial applications, J. Ind. Textil. 51 (5_suppl) (2022) 9047S–9070S.
[57] H. El-Dessouky, et al., Design, weaving and manufacture of a large 3D composite structures for automotive applications, in: 7th World Conference 3D Fabrics and their applications. 3D Fabrics and their,applications, 2016, pp. 123–132.
[58] M. Lefebvre, B. Francois, C. Daniel, Influence of high-performance yarns degradation inside three-dimensional warp interlock fabric, J. Ind. Textil. 42 (4) (2013) 475–488.
[59] L. Tong, A. Mouritz, Chapter 2 manufacture of 3D fibre preforms. 3D fibre reinf, Polym. Compos. (2009) 13–46.
[60] F. Stig, S. Hallström, Influence of crimp on 3D-woven fibre reinforced composites, Compos. Struct. 95 (2013) 114–122.
[61] Y. Mahadik, S. Hallett, Effect of fabric compaction and yarn waviness on 3D woven composite compressive properties, Compos. Appl. Sci. Manuf. 42 (11) (2011) 1592–1600.